Polymer 50 (2009) 3396–3402

Contents lists available at ScienceDirect

Polymer

journal homepage: www.elsevier.com/locate/polymer

Conformational transition characterization of glass transition behavior of polymers

Rongliang Wu, Bin Kong, Xiaozhen Yang*

Beijing National Laboratory for Molecular Sciences (BNLMS), Joint Laboratory of Polymer Science and Materials, State Key Laboratory of Polymer Physics and Chemistry, Institute of Chemistry, Chinese Academy of Sciences, Beijing 100190, China

ARTICLE INFO

Article history:
Received 16 January 2009
Received in revised form
21 April 2009
Accepted 11 May 2009
Available online 19 May 2009

Keywords:
Conformational transition
Glass transition
Poly(vinylidene fluoride)

ABSTRACT

The conformational transition behavior of polymer in the amorphous state has been investigated through molecular dynamics simulations across the glass transition temperature (T_g). We find that the conformational transition, a localized and short time dynamics feature, crosses over different barrier heights when the system transforms from the molten state into the glass state and the barrier height in the glass state is markedly lower than that above T_g. In addition to the overall transition behavior, the specific transitions between the rotational isomeric states (RIS) g^+, t^-, t^+ and g^- are also investigated in detail. The populations of these specific transitions undergo considerable changes when the temperature decreases; meanwhile, the larger transition rates of the ending torsions get diminished. Besides the rate, the rotation degrees of the dihedrals during the transitions also change their distributions tremendously through T_g, below which most of the larger transition angles (50–100°) were inhibited remaining those sharply around 30°. This possibly explains why below T_g the conformational transition process has a lower effective barrier.

1. Introduction

The glass transition is a very old phenomenon. It is marked by drastic changes in the mechanical properties of the material from a rubbery, viscous amorphous solid to a brittle, glassy amorphous solid. While the nature of glass transition is still not clearly known and it remains a topic of intense experimental [1–5] and theoretical interest [1,2,6–8]. Common ways to account for the glass transition are based on the free volume effect [2], but recent experiments have shown that such explanation is not fundamentally sound [1,3]. At high temperatures, where ergodicity prevails, the dynamics are nearly homogeneous and the theories [9] based upon free volume effects can be reasonably successful, while at low temperatures, the dynamics get strongly heterogeneous and a distribution of local barrier heights can be generated [1,10]. The heterogeneity in dynamics has been evidenced to exist in polymer and super cooled liquids near the glass transition temperature (T_g) [1,4] that is the dynamics in some regions of the sample can be orders of magnitude faster than dynamics in other regions only a few nanometers away [1].

In addition to the commonly used characterization of T_g by the specific volume temperature dependence, numbers of studies predict T_g by ways of the self-diffusion coefficient and viscosity [2,11], heat capacity or coefficient of thermal expansion [12,13], and structural relaxations [15,16]. New methods [17,18] of T_g prediction have also emerged, and with fast development of computational power the prediction of T_g by molecular dynamics simulations is frequently seen [19,20]. Some other experiments focused on the investigation of the various local dynamics of polymer and super cooled liquids around T_g using low-frequency quasi-local vibrations, namely the "Boson peak" [2] and probe molecules [14].

In our opinion, the local segmental motions in polymers make substantial contributions to the macroscopic properties of the material, and the motions of single torsional bonds are basic to the dynamics of polymer chains. Such dynamics are closely related to the structural changes of polymers, especially around T_g. It has already been pointed out that the glass transition was at least in part due to torsional jumping [21]. But experiments can rarely offer atomistic views to the local chain motions or the rotational isomerization of polymers [22]. Molecular dynamics (MD) simulations have provided sufficient atomistic detailed information regarding the structural changes and the short time dynamics in amorphous polymers.

The conformational transition rate and transition correlation were mostly used to characterize the segmental dynamics. Helfand et al. [23] did pioneering work using Langevin dynamics to investigate the conformational transitions of polyethylene-like chains in

* Corresponding author. Tel.: +86 10 82618423; fax: +86 10 62571123.
E-mail address: yangx@iccas.ac.cn (X. Yang).

0032-3861/$ – see front matter © 2009 Elsevier Ltd. All rights reserved.
doi:10.1016/j.polymer.2009.05.013

solutions, and pointed out that the rotational motion of the transforming bond is accompanied by motions in neighboring bonds. The single barrier nature of the correlated transitions was pointed out by MD simulations of Boyd et al. [24] and they explained even though these dihedrals are correlated, the transitions are not simultaneous with respect to barrier crossings. MD simulations have also been performed on the conformational properties of realistic polymers such as polyethylene [24–29], polypropylene [30], *cis*-polyisoprene [31], 1,4-polybutadiene [32,33] and aromatic copolyesters [34]. However, the conformational transitions defined vary from each other. Liang et al. [30] systematically investigated the influence of rotational isomeric state (RIS) width on the transition behaviors of atactic polypropylene. The shallow jumps, which had broader windows of RIS ($>\pm 20^\circ$), were found to be significant in the characterization of the motion of polymer chains through T_g.

In the present study, MD simulations have been performed to investigate the details of conformational transitions in the partially fluorinated polymer, poly(vinylidene fluoride) (PVDF) in bulk amorphous state across T_g. To obtain reliable information on such atomistic motions in polymers, the force field used needs to give exact torsional potentials. Byutner and Smith [35] have recently performed extensive high-level quantum chemistry study on the conformational properties of the PVDF oligomers, and developed a classical potential force field [36], which accurately reproduced the conformational energetics and made the detailed MD investigations possible. PVDF and its copolymers have attracted extensive theoretical and technological interests [37–39] due to their unique piezoelectric and mechanical properties. The rapid changes in the torsional angles often lead to significant variation of electric polarization in crystalline or amorphous PVDF [40,41], and investigations on the detailed conformational transitions might shed some light on its unique properties and the molecular mechanism of glass transition.

2. Methods

2.1. Force field and simulation details

All simulations in the current study were carried out in GROMACS 3.3 [42]. The potential functions and parameters adopted are listed in Table 1. An additional 7th term C_6 was added to the Ryckaert–Bellemans [43] dihedral function in the source code so as to meet the need for the PVDF force field [36]. The potential curve obtained with this force field is compared with that of polyethylene (PE) in Fig. 1. Unlike polyethylene, PVDF has its RIS or potential minima at the gauche states (g^+ and g^-) around 54° and 306°, respectively. The trans state splits into two (t^+ and t^-) with a subtle barrier in between.

The chains simulated have repeat unit CF_3–$(CH_2$–$CF_2)_n$–CH_3 ($n = 21$) as the building blocks. All units were connected head to tail, neglecting the sequence defects which were estimated to occur in real polymers. The initial conformation of the chain was chosen to be all trans and the random structures were obtained from a single chain MD run of around 500 ps at 583 K, during which the structures with reasonable end-to-end distances were picked out. This procedure is similar with the random walk algorithm frequently used in coarse-grained simulations [20,44]. The initial system contained 64 such picked out chains with different conformations randomly placed in a large gaseous cubic box, and an NPT run was performed with periodic boundary conditions in *xyz* directions at the temperature of 583 K until density equilibration had been reached. After a further equilibration run of 500 ps, the system was annealed sequentially to lower temperatures ranging from 193 K to 553 K, and each was equilibrated for 3–5 ns at external pressures of

Table 1
Potential functions and parameters for PVDF.

Non-bonded	$U_{nb}(r_{ij}) = A\exp(-Br_{ij}) - C/r_{ij}^6 + 332.08q_iq_j/r_{ij}$			
	A (kJ/mol)	B (nm^{-1})	C (kJ·nm^6/mol)	q_i[a]
C–C	62 659.58	30.90	2.68E−03	–
H–H	11 085.93	37.40	1.14E−04	0.1988
F–F	568 111.90	45.46	4.44E−04	−0.2493
C–H	18 074.88	34.15	5.78E−04	−0.5722 (−0.6837)
C–F	188 673.30	38.18	1.09E−03	0.6732 (0.8351)
H–F	51 463.20	41.43	2.25E−04	–

Bonds[b]	$U_{bond}(r_{ij}) = \frac{1}{2}K_{bond}(r_{ij} - r_{ij}^0)^2$	
	K_{bond} (kJ/mol/nm^2)	r_{ij}^0 (nm)
C_H–H	274 135.68	0.1085
C_F–F	417 814.24	0.1357
C_F–C_H	258 487.52	0.1534

Bends	$U_{bend}(\Phi_{ijk}) = \frac{1}{2}K_{bend}(\Phi_{ijk} - \Phi_{ijk}^0)^2$	
	K_{bend} (kJ/mol/rad)	Φ_{ijk}^0 (deg)
F–C_F–F	1004.160	105.27
F–C_F–C_H	753.120	107.74
C_H–C_F–C_H	671.950	118.24
H–C_H–H	322.168	109.27
H–C_H–C_F	358.987	108.45
C_F–C_H–C_F	671.950	118.24

Torsions[c]	$U_{torsion}(\theta_{ijkl}) = \sum_{n=0}^{6} C_n\cos^n(\phi)$						
	C_0	C_1	C_2	C_3	C_4	C_5	C_6
C_F–C_H–C_F–C_H	7.657	15.313	−11.004	−41.924	1.841	28.451	3.347
F_C–C_F–C_H–C_F	3.180	9.288	3.682	−18.493	−9.707	9.707	3.347

[a] The charges in parenthesizes are for the end group carbon atoms.
[b] C_H specifies the carbon atoms connected to H, and C_F specifies the carbon atoms connected to F.
[c] The function for torsion has been transformed into the Ryckaert–Bellemans [43] format, and an additional term (C_6) was added to the GROMACS source code.

1 bar, subsequent production runs extended 4 ns. The equilibration of the systems was monitored by the densities and potential energies at all temperatures since the complete relaxation of chain structures cannot occur due to the formation of glasses at relatively low temperatures. The leap-frog algorithm with an integration time step of 1 fs was used and the trajectories were recorded every 0.1 fs. All bonds were constraint with the LINCS [45] algorithm. The Nose–Hoover [46] temperature coupling and Parrinello–Rahman [47] pressure coupling methods were used to control the temperature and pressure respectively. Non-bonded dispersion interactions were truncated at 0.9 nm and the long range electrostatic interactions were handled using the Particle Mesh Ewald (PME) method

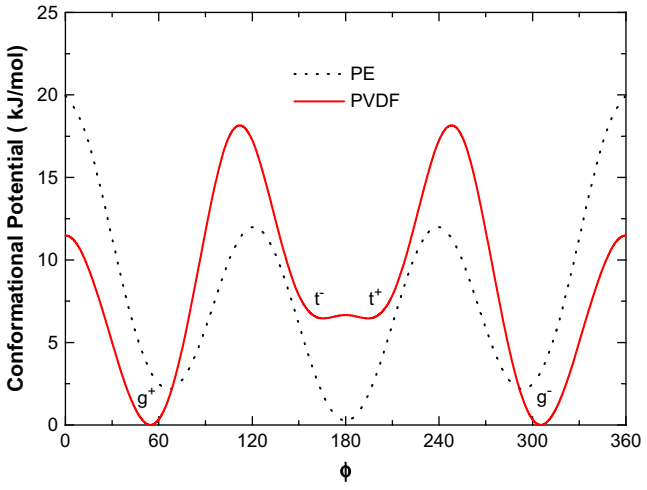

Fig. 1. Conformational potentials of PVDF and PE.

[48]. The long range dispersion corrections were also implemented for both energy and pressure accordingly.

2.2. The shallow jumps and the deep jumps

The determination of conformational transition varies in literature, for it depends crucially upon the time interval between comparing subsequent conformations and it also gives different results with different definitions of RIS [49]. The greater the time interval between sampling configurations, the smaller the number of barrier crossings will be counted since the torsions may cross and re-cross back without being detected. It was demonstrated that the lower limit on the time required for most re-crossings to take place was ~0.1 ps [49], which is exactly the time interval we keep for our trajectories. As for the RIS definition, some claimed that each transition should cross the torsional potential minima of both the before and the after states; Boyd et al. [24] proposed the criterion based on the dihedral angle being within a relatively narrow window of ±5° or ±10° to prevent the very short-lived over-and-back transitions; Takeuchi and Roe [56] accepted a transition if the dihedral angle crossed top of the potential barrier; and Sumpter et al. [50] counted transitions when the dihedral angles rotate more than 90°. Previous work in our group [30] defined the transitions according to the width at the barrier top (W) and made clear distinction between the shallow jumps ($W < 40°$) and the deep jumps ($W > 40°$) as defined therein. This earlier work tested all criteria of conformational transition in analyzing a series of MD runs through T_g. It was found that the shallow jumps recognize T_g clearly [30].

In the present work, the shallow jump is accordingly defined as crossing the barrier top by 10° and the deep jump is defined as transitions from the potential minima (±10°) of one RIS to other counterparts. The RIS (g^+, t^-, t^+ and g^-) for shallow jumps are 10–100°, 120–180°, 180–240°, 260–350° and for deep jumps are 44–64°, 156–180°, 180–204°, 296–316°. The shallow jumps involve the case that the transition occurrences are located close to the top of the barrier, which is not involved in the deep jumps. Any transitions between the RIS were recorded and the transition rate k_t (i → j) from state i to j is defined as

$$k_t(\mathrm{i}\rightarrow\mathrm{j}) = \frac{N_t}{\phi_i N t_s}, \tag{1}$$

where N_t is the total number of transitions from state i to j during the sampling time t_s, N is the total number of backbone dihedrals in the system, ϕ_i is the fraction of dihedrals in state i. The $t^+ \leftrightarrow t^-$ transitions are not taken into account since their values are orders of magnitude larger than others. A representative time evolution of a torsion angle is shown in Fig. 2 in accompany with the jump definitions. The shallow jumps encompass most of the fluctuations while the deep jumps neglect some of the short-lived transitions and many of these short-lived transitions also pass the potential minima.

3. Results and discussion

3.1. Glass transition temperature and local structure

The volume–temperature relationship is often used to locate the volumetric glass transition temperature (T_g). The specific volumes of bulk PVDF as well as their standard deviations are plotted against temperature in Fig. 3. The solid lines are linear fits and they intersect around 340 K, which is within the glass transition range in experiments (233–371 K) [51]. While this temperature is believed to be much higher than the realistic polymer at such a short chain length, for our annealing speed is much faster than can be implemented in

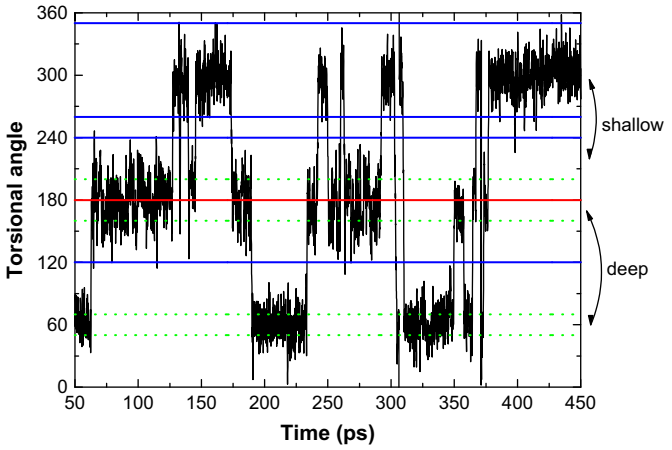

Fig. 2. Time evolution of a torsional angle and the definitions for deep and shallow jumps.

experiments. Above T_g, the specific volumes correspond very well with experiments [52]. The expansion coefficients are slightly larger above T_g (4.95×10^{-4} K^{-1}) and smaller below T_g (5.25×10^{-5} K^{-1}) than experiments [51] (3.60×10^{-4} K^{-1}; 7.90–14.10 $\times 10^{-5}$ K^{-1}). In addition, around the experimental melting point (~420 K) [52], no inconsistent variations are observed, showing the absence of crystallization.

The local structure can be well characterized by the radial distribution function (RDF) shown in Fig. 4 and the characteristic ratio C_n in Fig. 5. At temperatures above and below T_g, the RDF appears similar in shape with each other, and except the local conformations no long range ordering can be designated. The characteristic ratio C_n offers local chain structures

$$C_n = \left\langle R^2(n) \right\rangle \Big/ nl^2, \tag{2}$$

where $R^2(n)$ is the square internal distance between backbone carbons separated by n bonds, the angle bracket denotes ensemble average over all atom pairs, l is the backbone bond length. At all temperatures, C_n increases smoothly with n until plateau values ~40, which demonstrates that the chains are in the amorphous state. Especially at the θ temperature (463 K), C_n has plateau value of ~5.8, which is in good agreement with the experimental value of 5.6 ± 0.3 [53].

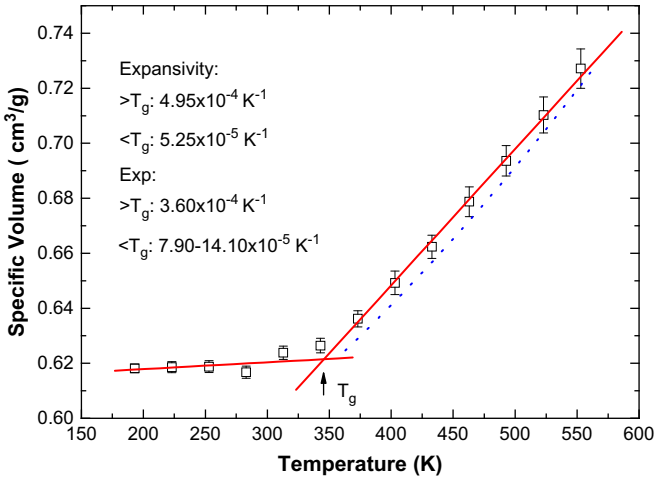

Fig. 3. Specific volumes of amorphous PVDF obtained from NPT simulations. Solid lines are linear fits, and the dashed line represents the experimental values [52].

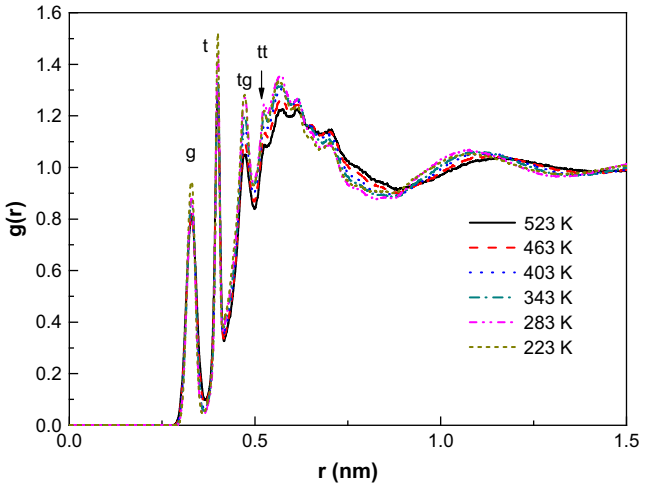

Fig. 4. Radial distribution functions between carbon atoms at selected temperatures. The functions are plotted without consideration of the connected pairs of bonds and angles.

3.2. The transition barriers before and after T_g

The transition state theory (TST) of chemical reactions was utilized by Chandler [54] to investigate the statistics of internal rotation dynamics. One of the most common forms of the theory is

$$k = \frac{k_B T}{h} e^{-\Delta G^{\dagger}/RT}, \quad (3)$$

where $\Delta G^{\dagger}$ is the Gibbs free energy of activation, k_B is the Boltzmann constant, and h is the Planck constant. While the Arrhenius equation has been used more frequently [24,26,34]

$$k_t = A \exp\left(-\frac{E_a}{RT}\right) \text{ or } \ln k_t = -\frac{E_a}{R}\frac{1}{T} + \text{const.}, \quad (4)$$

where E_a represents the activation energy of conformational transition, R is the ideal gas constant. In fact, the free energy involved in TST is itself temperature dependent. In addition, the TST divides the entire process into two stages, one is the formation of the transition state (the exponential term), which needs an activation energy E_a; and the other is the production stage from the transition state (k_BT/h) [55]. For a conformational transition especially the deep jumps from one RIS to another, to cross the barrier is the most crucial for the entire process, while the latter stage can be regarded as diffusion term and no barrier is involved. Thus the exponential term (with a similar form with the Arrhenius equation) suffices for the description of the energy barriers involved in shallow jumps. But for the deep jumps, they involve not only the barrier crossing process but also the diffusion from the transition state to the potential minima. TST might offer better description on the deep jumps. To obtain the barrier height, it is usually easier to perform Arrhenius plot (logarithm of rate versus reciprocal temperature) and calculate the barrier energy from the slope. Therefore, shallow jumps are good for obtaining reasonable barrier energy. This idea will be further validated below.

The overall transition rates of both the deep and the shallow jumps for PVDF are plotted against temperature in Fig. 6(a). It seems that the two sorts of transition rates show similar temperature relationship. The salience found in our previous paper for atactic polypropylene [30] is not clearly distinguishable for PVDF. The transition at high temperatures is much more temperature dependent than that of polypropylene, which has side groups retarding the transitions. In the present study, we plotted logarithmic rate vs. inverse temperature in Fig. 6(b) and we found that slope changes around 310 K. T_g obtained from the conformational transition rates is

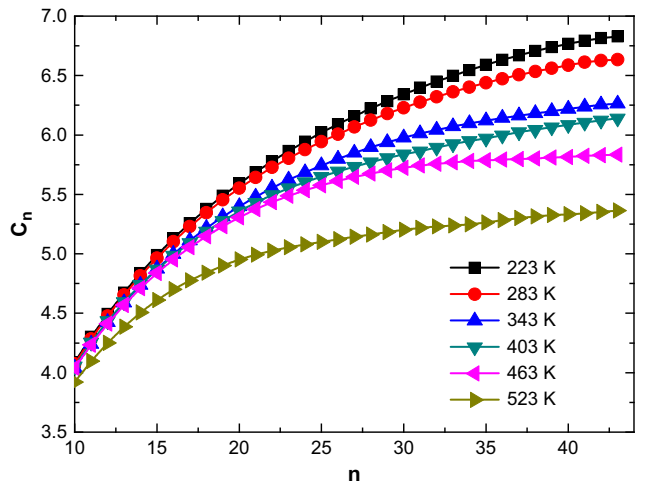

Fig. 5. Equilibrium characteristic ratios along the chains at selected temperatures.

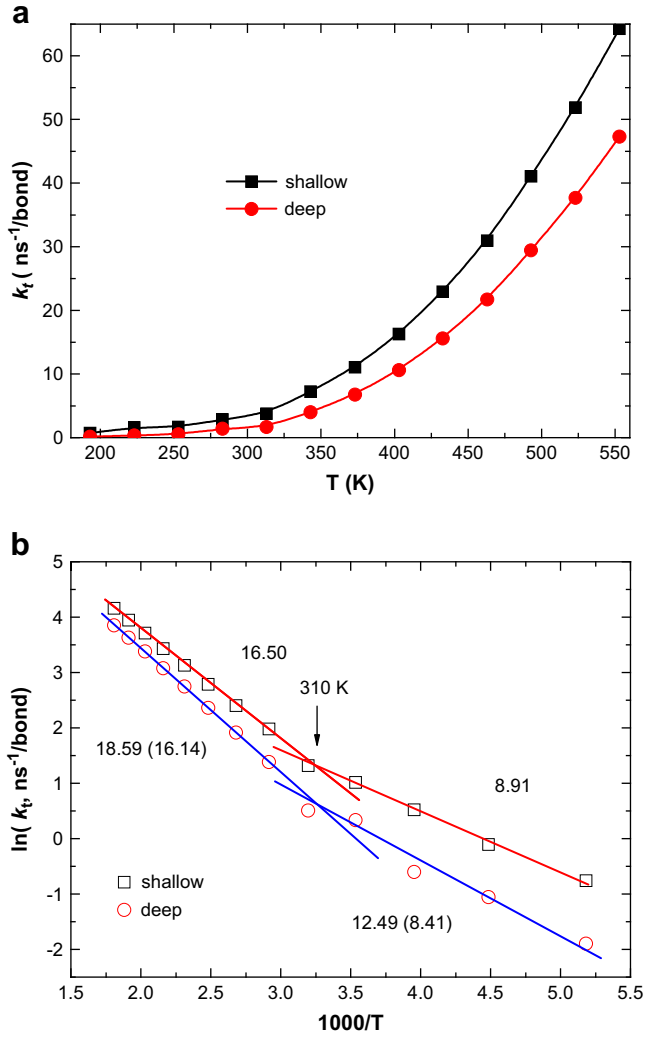

Fig. 6. Temperature dependences of the overall conformational transition rates for both deep and shallow jumps across T_g. The activation energies denoted are in kJ/mol and the values in parenthesis are the activation energies fitted according to TST (Eq. (3)): (a) overall rates vs. temperature, (b) logarithmic rates vs. inverse temperature.

more accurate and lower than that from the volumes. This is because that the two measurements regard different relaxation behaviors. Thermodynamically, the former is based on equilibrium of local conformations and the latter on equilibrium of long scale structures. Though there exists difference, this is the characterization of T_g through the window of conformational transition behavior, and it is developed from our previous work [30].

At temperatures higher than T_g, the perfect linear relationship shows good Arrhenius behavior for both jumps as was found by others [24,26,27,56]. The deep jumps and the shallow jumps give activation energies of 18.59 kJ/mol and 16.5 kJ/mol, both are larger than that of PE (14.8 kJ/mol)[24]. As already referred to, the TST might give better description on the deep jumps, the activation energy obtained by fitting Eq. (3) to the same transition rates is 16.14 kJ/mol, which agrees well with that obtained from the shallow jumps. This in turn further proves that the use of shallow jump is reasonable. When the temperature gets further decreased to below 310 K, the overall transition rates do not follow the previous lines but appear orders of magnitude larger than expected, and the activation energy reduces significantly in the glass state. For the deep jumps, the activation energy obtained from TST (8.41 kJ/mol) also agrees well with that of the shallow jumps 8.91 (kJ/mol) below T_g. The deep jumps overestimate the transition barrier if Arrhenius equations were used.

In the present study, we found before and after T_g the transition barrier heights are considerably different. Arrhenius plots show the turning point is around T_g. It may be contributed to different structural environments in both states. Especially, we found the barrier height is lower in the glass state than that in the molten state. This phenomenon is clearly observed in the present study and hard to be explained by using the free volume theory. In latter sections, we discussed and interpreted this phenomenon with obtained results.

3.3. The specific transitions and barriers

The overall transitions include the specific transitions of $g^+ \leftrightarrow g^-$, $g^+ \rightarrow t^-$, $t^- \rightarrow g^+$, $g^- \rightarrow t^+$ and $t^+ \rightarrow g^-$. The specific transition rates, which take into account the average population of dihedrals in the pre-state of a transition (see Eq. (1)), are plotted in Fig. 7, where $g \rightarrow t$ and $t \rightarrow g$ are averages of $g^+ \rightarrow t^-$ and $g^- \rightarrow t^+$, $t^- \rightarrow g^+$ and $t^+ \rightarrow g^-$, respectively. Table 2 shows the activation energies of the specific transitions $g^+ \leftrightarrow g^-$, $g \rightarrow t$, $t \rightarrow g$, E_a have values of 15.39, 16.34, and 15.87 kJ/mol above T_g and 10.95, 9.32, and 9.10 kJ/mol below T_g, respectively. As is the same with the overall transitions, the barriers decrease significantly when entering the glass state.

Table 2
Activation energies for the conformational transitions.

	E_a (kJ/mol)		Fractions in the overall transitions	
	$<T_g$	$>T_g$	223 K	403 K
$g^+ \leftrightarrow g^-$	10.95	15.39	0.16	0.34
$g \rightarrow t$	9.32	16.34	0.42	0.33
$t \rightarrow g$	9.10	15.87	0.42	0.33

In general, the barrier is from free energy surface of a kinetic process, not only from potential energy. However, it is usually easier to refer to the potential curve in Fig. 1. This curve gives $g^+ \leftrightarrow g^-$, $g \rightarrow t$ and $t \rightarrow g$ barriers of 11.5, 18.2, and 11.7 KJ/mol. In the present study, we measured kinetically the barrier heights in various cases even for the specific transitions as shown in Table 2. The data show differences between the one from the potential and the one from kinetics measurement. Especially interesting is the energy difference from $g \rightarrow t$ and $t \rightarrow g$. The result shows that the difference is 6.5 kJ/mol in the potential curve and 0.2–0.5 kJ/mol from kinetically measurement. The former gives such big value since the potential curve is of thermodynamics in nature instead of kinetics.

Besides the activation energy changes around T_g, the specific transitions show another indication: populations of the specific transitions have a considerable variation in the two states as shown in Fig. 8 and Table 2. At high temperatures the three transitions show much close populations. For $g \rightarrow t$ or $t \rightarrow g$ the fractions are ~34% and that of $g^+ \leftrightarrow g^-$ is ~32%. When temperatures is decreased, the fraction of the $g^+ \leftrightarrow g^-$ transition poses slight increase followed with drastic descent, at the meantime, the fractions of $g \rightarrow t$ and $t \rightarrow g$ transitions change in the opposite direction. The specific transition with the smallest activation energy ($g^+ \leftrightarrow g^-$) among the three becomes the one with largest activation energy. This simply indicates that in the two states the local structures of the system regarding the transition environments are substantially altered.

3.4. Distribution of conformational transition rates along the chain

The overall transition rates k_t of each bond averaged from the 64 chains are plotted against the torsion numbers in Fig. 9. At high temperatures, the ending dihedrals exhibit around two times larger

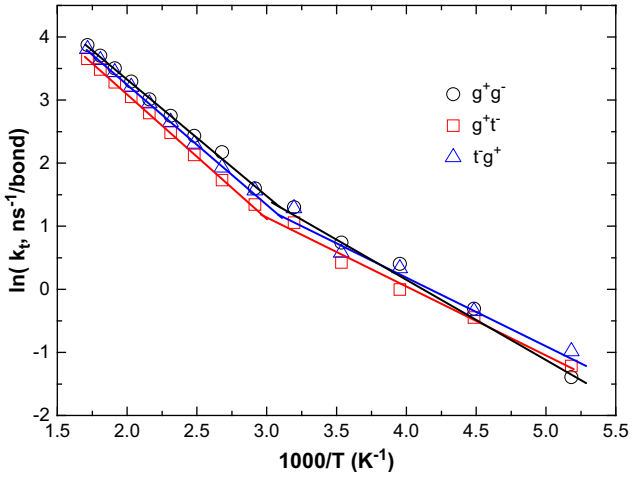

Fig. 7. Temperature dependences of the specific transition rates, i.e. the $g^+ \leftrightarrow g^-$, $g \rightarrow t$ and $t \rightarrow g$ transitions.

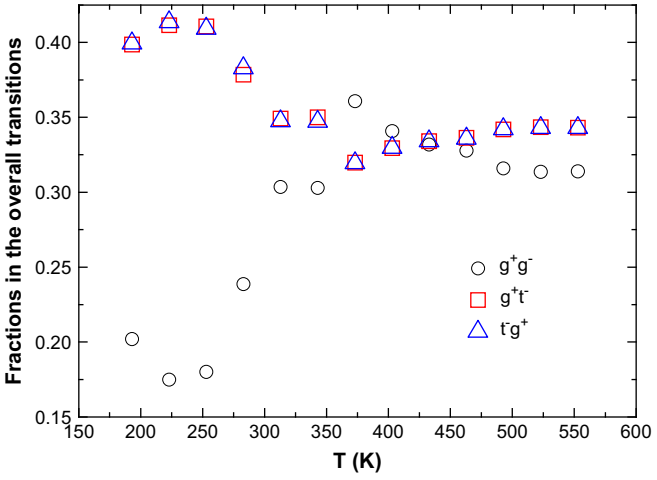

Fig. 8. Fractions of the contribution of the specific transitions to overall transitions.

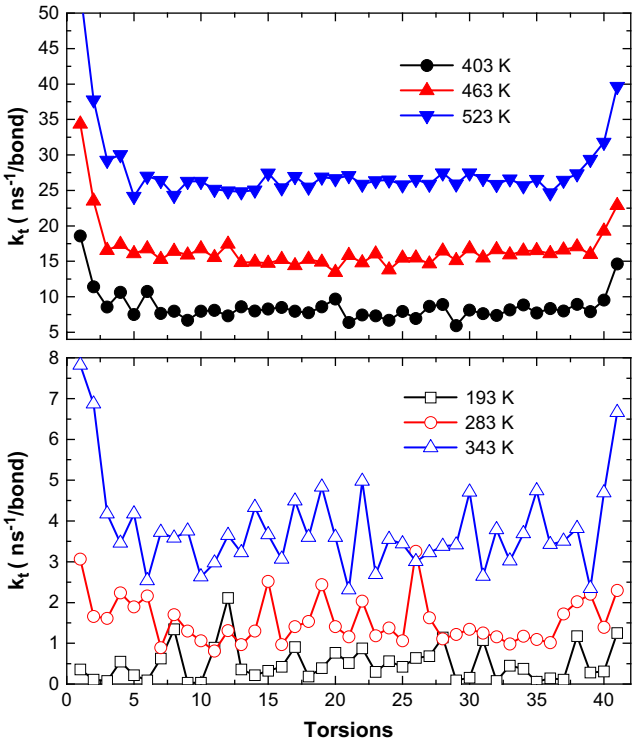

Fig. 9. Average transition rates along the chains. The chain end effect is prominent above T_g, but gets diminished at low temperatures.

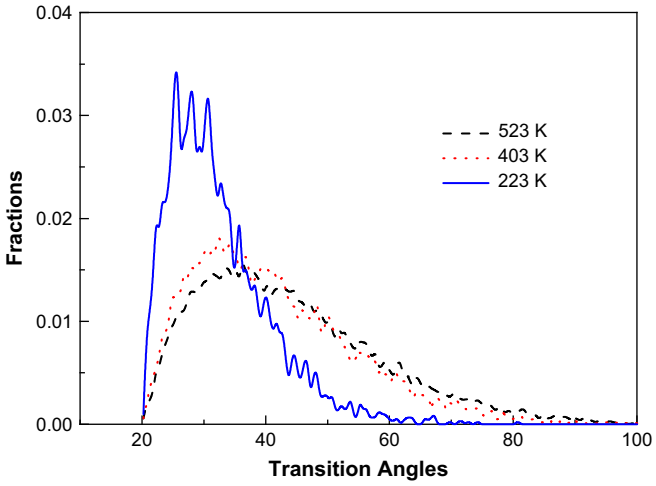

Fig. 10. Distributions of transition angles for all jumps.

transition rates relative to those interior to the chains. In addition, the different ending groups also have much influence on the transition rates. The dihedral numbered 1 has CH_3 as the end group while the end group of the dihedral at the other end of the chain is CF_3. The dihedrals ending with CH_3 at the terminus have larger transition rates than those with CF_3 at the terminus. The larger group size and polarizability of the fluorine atoms might probably be the reason.

When temperature is decreased, mobility of the chains depicted by conformational transition rate shows remarkable changes: 1) the large difference between the rates of the ending and the interior torsions disappeared; 2) the even distribution of transition rates (with deviations of ~10%) becomes much more heterogeneous (with a huge deviation of ~80%). This heterogeneous distribution reveals that in the glass state the conformational transition rates appear somewhere higher and somewhere lower. The slow mode might possibly serve as the microscopic mechanism of the long chain segment motion being "frozen" under T_g in the view of conformational transitions.

3.5. The inhibition of larger magnitude transition dihedrals

The details of conformational transitions can be monitored by the transition angles, defined as the angular degrees a dihedral sweeps over during a transition. More specifically, the angle was measured as a difference between the departure dihedral angle and the arrival dihedral angle of torsion during a transition. The departure dihedral angle is the last position in the before RIS, and the arrival dihedral is the first landing position in the after RIS. Evidently, the magnitude of the transition angle depends on the activation energy of a transition. Their distributions for all jumps at three selected temperatures are plotted in Fig. 10. At high temperatures, most of the transitions sweep around 37° with a broad distribution in the large degree side. But when the temperature is decreased below T_g, the distribution gets significantly sharper, most of which sweep less than 30°. Half width of the distribution narrows from ~30° to less than 15°. A huge amount of populations from 50° to 100° become highly inhibited.

We found that the polymer in the glass state loses the large angle transitions and possesses only small magnitude transitions, which results in a possible explanation of the lower transition barrier below T_g. Generally, the activation energy for conformational transition of each torsion would not be everywhere the same, it may have a distribution[1,10]. Boyd and Smith's simulation study [10] indicated that the transition barrier heights have a distribution with width of about ±15 kJ/mol around 200 K for polyethylene. One can thus consider that at higher temperature the higher and the lower barriers can all be crossed in conformational transitions, which is supported by the above data having broad transition angle distribution above T_g, since the higher activation energy corresponds to the larger transition angle. In the glass state, the system loses the larger transition angles which originate from loss of the higher activation energy in the system. With lower activation energies, only low transition barriers can be crossed in the glass state. This possibly explains the transition barriers decrement under T_g in Table 2 to a certain extent.

As already found below T_g the local dynamics get substantially activated and some torsions have transition rates orders of magnitude higher than expected. These activated torsions were supposed small magnitude transitions in Fig. 10 and an activated dynamics mechanism was assumed by Boyd and Smith [26]. They thought that in glasses where the dynamics get severely retarded, overpopulation of torsions divergent from the potential minima is located and the residence times at these sites are so long that the bonds can be considered to be trapped. These torsion sites may become eligible centers for the conformational transitions, which results in the reduced effective barrier [26]. In the present study, our result of the transition dihedral indicates that in the glass state the conformational transition behavior becomes jumping a very small step, about 30°. This result supports the above mechanism. It should be noted here that the number of activated torsions is still quite minor although they make major contributions to the system dynamics. Most of the torsions are still trapped within the RIS bottom, generally attributed to the 'frozen' of local conformational structure or environment.

4. Conclusions

MD simulations have been performed on amorphous PVDF using a high-level quantum chemistry force field [36] through the glass transition temperature. The shallow jumps are found to be a better choice for description of conformational transitions than the deep jumps, which overestimate the transition barrier if the Arrhenius equation is used. It was found that when the system transforms from the melt to the glass state the overall conformational transitions cross over different barriers: 16.5 KJ/mol and 8.91 KJ/mol, respectively. The specific transitions show similar behaviors and in addition, a huge amount of the transition angles from 50° to 100° was found to be inhibited in the glass state, namely the dihedrals only perform the small magnitude transitions. Evidently, in this situation conformational transitions that can be realized are those across lower barriers. This is possibly the reason for the decrease of the transition barriers in the glass state. In the present study, we have found that the conformational transition is a very important property describing the local dynamics in polymers around T_g.

Acknowledgements

We acknowledge the support from National Science Foundation of China (90612015, 20474073, 20490220, 20674090), and 973 (2004CB720606) projects.

References

[1] Ediger MD. Annu Rev Phys Chem 2000;51:99–128.
[2] Angell CA. Proc Natl Acad Sci 1995;92:6675–82.
[3] Ferrer ML, Lawrence C, Demirjian BG, Kivelson D, Alba-Simionesco C, Tarjus G. J Chem Phys 1998;109(18):8010.
[4] Sillescu HJ. Non-Cryst Solids 1999;243:81–108.
[5] Chaudhuri P, Berthier L, Kob W. Phys Rev Lett 2007:99.
[6] Adam G, Gibbs JH. J Chem Phys 1965;43(1):139–46.
[7] Gotze W, Sjogren L. Rep Prog Phys 1992;55:241–376.
[8] Jérôme B, Commandeur J. Nature 1997;386:589–92.
[9] Angell CA, Ngai KL, McKenna GB, McMillan PF, Martin SW. J Appl Phys 2000; 88(6):3113–57.
[10] Boyd R, Smith G. Polymer dynamics and relaxation. New York: Cambridge University Press; 2007.
[11] Swallen SF, Bonvallet PA, McMahon RJ, Ediger MD. Phys Rev Lett 2003; 90(1):015901.
[12] Riha P, Hadac J, Slobodian P, Sáha P, Rychwalski RW, Kubát J. Polymer 2007;48(25):7356–63.
[13] Campbell CG, Vogt BD. Polymer 2007;48(24):7169–75.
[14] Park J-W, Ediger MD, Green MM. J Am Chem Soc 2001;123(1):49–56.
[15] Svoboda R, Pustková P, Málek J. Polymer 2008;49(14):3176–85.
[16] Pawlus S, Kunal K, Hong L, Sokolov AP. Polymer 2008;49(12):2918–23.
[17] Bertinetto C, Duce C, Micheli A, Solaro R, Starita A, Tiné MR. Polymer 2007; 48(24):7121–9.
[18] Schut J, Bolikal D, Khan IJ, Pesnell A, Rege A, Rojas R, et al. Polymer 2007; 48(20):6115–24.
[19] Zheng ZMAWT, Jiang Q. Polymer 2008;49(16):3578–81.
[20] Bulacu M, Giessen Evd. Phys Rev E 2007;76:011807.
[21] Loncharich RJ, Brooks BR. J Mol Biol 1990;215:439–55.
[22] Zheng J, Kwak K, Xie J, Fayer MD. Science 2006;313:1951–5.
[23] Helfand E, Wasserman ZR, Weber TA. J Chem Phys 1979;70(4):2016–7.
[24] Boyd RH, Gee RH, Han J, Jin Y. J Chem Phys 1994;101(1):788–97.
[25] Jin Y, Boyd RH. J Chem Phys 1998;108(23):9912–23.
[26] Bharadwaj RK, Boyd RH. J Chem Phys 2001;114(11):5061–8.
[27] Canales M, Sesé G. J Chem Phys 2006;125(5):054906.
[28] Karatasos K, Adolf DB, Hotston S. J Chem Phys 2000;112(19):8695–706.
[29] Zúñiga I, Bahar I, Dodge R, Mattice WL. J Chem Phys 1991;95(7):5348–54.
[30] Liang T, Yang Y, Guo D, Yang X. J Chem Phys 2000;112(4):2016–20.
[31] Fukuda M, Kikuchi H. J Chem Phys 2000;113(10):4433–43.
[32] Kim E-G, Mattice WL. J Chem Phys 1994;101(7):6242–54.
[33] Smith GD, Borodin O, Paul W. J Chem Phys 2002;117(22):10350–9.
[34] Bharadwaj R, Boyd RH. J Chem Phys 1999;110(20):10203–11.
[35] Byutner OG, Smith GD. Macromolecules 1999;32(25):8376–82.
[36] Byutner OG, Smith GD. Macromolecules 2000;33(11):4264–70.
[37] Carbeck JD, Rutledge GC. Polymer 1996;37(22):5089–97.
[38] Carbeck JD, Rutledge GC. Macromolecules 1996;29(15):5190–9.
[39] Salimi A, Yousefi AA. J Polym Sci Part B Polym Phys 2004;42(18):3487–95.
[40] Abe Y, Tashiro K, Kobayashi M. Comput Theor Polym Sci 2000;10(4):323–33.
[41] Karasawa N, Goddard WA. Macromolecules 1995;28(20):6765–72.
[42] Spoel Dvd, Lindahl E, Hess B, Groenhof G, Mark AE, Berendsen HJC. J Comput Chem 2005;26(16):1701–18.
[43] Ryckaert JP, Bellemans A. Faraday Discuss Chem Soc 1978;66:95–106.
[44] Auhl R, Everaers R, Grest GS, Kremer K, Plimpton SJ. J Chem Phys 2003; 119(24):12718–28.
[45] Hess B, Bekker H, Berendsen HJC, Fraaije JGEM. J Comput Chem 1997; 18(12):1463–72.
[46] Nosé S. Mol Phys 1984;52(2):255–68;
Hoover WG. Phys Rev A 1985;31:1695–7.
[47] Parrinello M, Rahman A. J Appl Phys 1981;52(12):7182–90.
[48] Darden T, York D, Pedersen L. J Chem Phys 1993;98(12):10089–92.
[49] Brown D, Clarke JHR. J Chem Phys 1990;92(5):3062–73.
[50] Sumpter BG, Noid DW, Wunderiich B. J Chem Phys 1990;93(9):6875–89.
[51] Brandrup J, Immergut EH, Grulke EA. Polymer handbook. 4 ed. New York: Wiley-Interscience; 2003.
[52] Nakagawa K, Ishida Y. Colloid Polym Sci (Kolloid-ZZ Polym) 1973;251(2):103–7.
[53] Welch GJ. Polymer 1974;15(7):429–32.
[54] Chandler D. J Chem Phys 1978;68(6):2959–70.
[55] Eyring H. J Chem Phys 1935;3(2):107–15.
[56] Takeuchi H, Roe R-J. J Chem Phys 1991;94(11):7458–65.